Moving toward Subkilometer Modeling Grid Spacings: Impacts on Atmospheric and Hydrological Simulations of Extreme Flash Flood–Inducing Storms

NIKOLAOS S. BARTSOTAS AND EFTHYMIOS I. NIKOLOPOULOS

Atmospheric Modeling and Weather Forecasting Group, Department of Physics, National and Kapodistrian University of Athens, and Innovative Technologies Center SA, Athens, Greece

EMMANOUIL N. ANAGNOSTOU

Civil and Environmental Engineering, University of Connecticut, Storrs, Connecticut

STAVROS SOLOMOS

Institute for Astronomy, Astrophysics, Space Applications and Remote Sensing, National Observatory of Athens, Athens, Greece

GEORGE KALLOS

Atmospheric Modeling and Weather Forecasting Group, Department of Physics, National and Kapodistrian University of Athens, Athens, Greece

(Manuscript received 11 April 2016, in final form 13 October 2016)

ABSTRACT

Flash floods develop over small spatiotemporal scales, an attribute that makes their predictability a particularly challenging task. The serious threat they pose for human lives, along with damage estimates that can exceed one billion U.S. dollars in some cases, urge toward more accurate forecasting. Recent advances in computational science combined with state-of-the-art atmospheric models allow atmospheric simulations at very fine (i.e., subkilometer) grid scales, an element that is deemed important for capturing the initiation and evolution of flash flood–triggering storms. This work provides some evidence on the relative gain that can be expected from the adoption of such subkilometer model grids. A necessary insight into the complex processes of these severe incidents is provided through the simulation of three flood-inducing heavy precipitation events in the Alps for a range of model grid scales (0.25, 1, and 4 km) with the Regional Atmospheric Modeling System–Integrated Community Limited Area Modeling System (RAMS–ICLAMS) atmospheric model. A distributed hydrologic model [Kinematic Local Excess Model (KLEM)] is forced with the various atmospheric simulation outputs to further evaluate the relative impact of atmospheric model resolution on the hydrologic prediction. The use of a finer grid is beneficial in most cases, yet there are events where the improvement is marginal. This underlines why the use of finer scales is a step in the right direction but not a solitary component of a successful flash flood–forecasting recipe.

1. Introduction

Flood forecasting has steadily remained in the epicenter of research during the last decades for a plausible amount of reasons. A changing climate has induced a growing number of areas to be affected by heavy precipitation events (HPEs; Simonović 2003). Large rainfall accumulations (>100 mm) over short time periods often lead to flash flooding incidents that are associated with devastating societal and economic impacts (Jonkman 2005; Bouilloud et al. 2010; Doocy et al. 2013). Despite the advancements in weather monitoring and forecasting allowing for a better understanding of the fine mechanisms of these events, their predictability remains a particularly challenging task.

The root cause of the predictability uncertainty lies in the small spatiotemporal attributes that characterize their development and evolution (Weckwerth et al.

Corresponding author e-mail: George Kallos, kallos@mg.uoa.gr

DOI: 10.1175/JHM-D-16-0092.1

2014). Especially over mountainous and generally complex terrain areas, the triggering of terrain-induced disturbances and establishment of meso- and local-scale flows result in exaggerated spatial distributions of rainfall (Smith et al. 1997). It comes as no surprise that typically encountered limitations in flash flood forecasting, such as incorrect positioning of convective precipitation or vague estimations of high rainfall values (Fritsch and Carbone 2004), exhibit an amplified form over such areas.

The Alps constitute an ideal study area for the investigation of HPEs that induce major flash flooding incidents. When synoptic conditions favor the transfer of humid air masses from the Mediterranean Sea, the effect of orographic enhancement on precipitation often results in large amounts of rainfall that accumulate within a short timeframe over small basins with short response times to precipitation. A number of international research programs and field campaigns have focused on the study and analysis of hydrometeorological extremes in the mountainous areas, including the Mesoscale Alpine Programme (MAP; Bougeault et al. 2001; Rotunno and Houze 2007), the Convective and Orographically Induced Precipitation Study (COPS; Wulfmeyer et al. 2011), and the Hydrological Cycle in the Mediterranean Experiment (HyMeX; Drobinski et al. 2014; Ducrocq et al. 2014).

Numerical weather prediction (NWP) constitutes a cornerstone in flash flood forecasting, as it provides the driving input to flood modeling. The representation of cloud formation and development in atmospheric models is strongly related to the modeling grid resolution. Explicit resolving of mesoscale convective systems often requires a grid spacing of 2 km or finer, implying a consequential dramatic increase in computational cost. This is the main reason why global and some regional scale models still rely on convective parameterization schemes for the description of convective processes. However, recent advances in computational science permit cloud-resolving configurations in regional forecasting models, at least for limited areas of increased interest. This is an important step for providing more accurate simulations of extreme weather events. A plausible speculation, though, involves the definition of the scale where benefits no longer commensurate the extra computational cost or other drawbacks, for example, generation of truncation errors over steep terrain (Janjić 1977; Mahrer 1984; Smith et al. 1997; Fuhrer 2005). Therefore, adoption of finer scales and the relevant modeling results need to be well understood through careful evaluation against observations.

A number of past works have focused on the effect of model grid resolution on the simulation of heavy precipitation events. Bernardet et al. (2000) simulated multiple convective events, with the highest model resolution reaching 1.6 km, and concluded that a fine grid with spacing on the order of 2 km was sufficient to capture convection. Schwartz et al. (2009) compared precipitation forecasts between 2- and 4-km model resolutions and showed that while 2-km forecasts produced more detailed structures on the smallest resolvable scales, the initiation and evolution of convection were remarkably similar to the 4-km output. Buzzi et al. (2014) presented comparisons from a regional model for grid scales ranging between 1 and 3 km and found that representation of precipitation magnitude and spatial location was improving with increasing resolution. The 1-km grid spacing was the scale where improved results emerged in a number of studies on precipitation over mountainous terrain (Colle and Mass 2000; Colle et al. 2005; Schwartz 2014). Furthermore, other researchers (e.g., Roberts et al. 2009; Davolio et al. 2015) have additionally investigated the hydrologic impact of using atmospheric grid spacing down to 1 km and showed consistently increasing improvement in flood prediction with increasing resolution.

This work builds along the same line of thought and expands, relative to past work, in two main aspects. First, investigation extends to subkilometer model resolution in an attempt to identify if further benefits or potential limits exist in the improvements due to finer resolution reported in past work. Second, the impact of model resolution is examined with respect to precipitation type (convective/stratiform) to identify potential dependences. A state-of-the-art, high-resolution integrated atmospheric model [Regional Atmospheric Modeling System–Integrated Community Limited Area Modeling System (RAMS–ICLAMS); Solomos et al. 2011; Kushta et al. 2014] is used to simulate three major flash flood events (two convective and one of stratiform type) in subkilometer grid scales. To understand the impact of grid scale, different model setups with respective inner domain grid spacings of 4, 1, and 0.25 km are used to resolve precipitation-related mechanisms such as deep convection and low-level convergence over mountainous Alpine terrain. Finally, the impact of atmospheric model resolution on flash flood simulation accuracy is assessed based on a distributed hydrological model that is used to simulate basin flood response to the various precipitation forcing datasets. Model simulations are compared to high-resolution, gauge-adjusted radar rainfall fields, and attainable benefits from the adoption of very fine grid scales in models are thoroughly discussed.

In the following section, we present an overview of the study area, the NWP, and the hydrological model setup as well as a description of the datasets that were used.

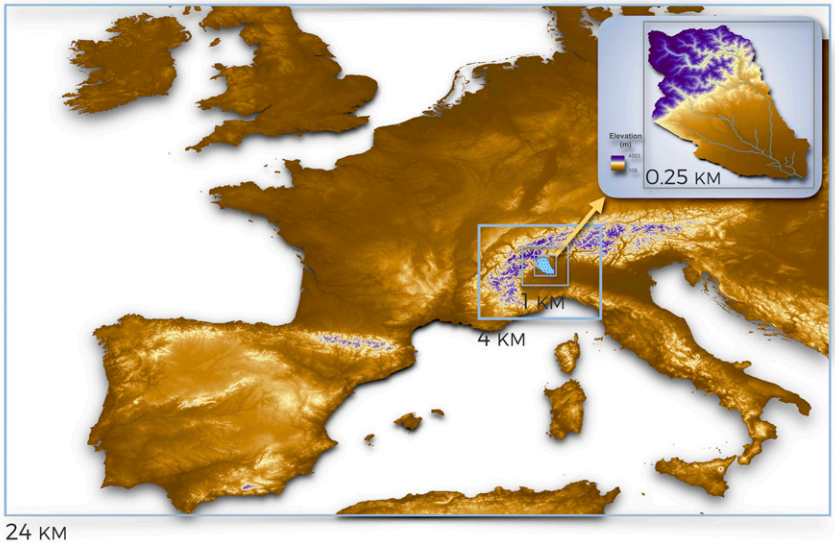

FIG. 1. Study area in the Sesia River basin in northern Italy. The 24-, 4-, 1-, and 0.25-km model grids are displayed.

The methodology is described in section 3, and the analyses of the events and results are presented in section 4, followed by a discussion section. Conclusions are summarized in section 5.

2. Study area and data

a. Study area

The selection process of a suitable test bed for the simulations was tied to an array of aspects that had to be fulfilled. Foremost, the ground characteristics had to comply with the archetype of complex terrain areas. In addition to that, the availability of an accurate rainfall estimate dataset over the area that would serve as the ground truth was essential in order to properly evaluate the modeling outputs. A broad number of documented flash flood incidents over this area allowed for a verification process under diverse storm characteristics.

The Alpine river basin of Sesia closed at Palestro in the northwestern part of Italy (Fig. 1) complied with all the aforementioned criteria. It features an elevation range that varies from 108 to 4555 m within a drainage area of 2587 km^2. Doppler radar data are available at high spatial (1 km) and temporal (10 min) resolutions, constituting an accurate precipitation dataset that can serve as ground reference for verification (Sangati et al. 2009). Finally, a number of HPEs have triggered major flash flooding episodes in recent years. A selection of three distinct flood-inducing HPEs (2002, 2005, and 2006) was made based on their severity and physical characteristics (Table 1). A detailed analysis of each selected event is presented in section 4a.

b. Description and setup of the atmospheric model

For the simulation of the HPEs, the integrated atmospheric model RAMS–ICLAMS (Solomos et al. 2011; Kushta et al. 2014) was used. The model was developed by the Atmospheric Modeling and Weather Forecasting Group at the University of Athens as an enhanced version of RAMS, version 6.0 (Pielke et al. 1992; Cotton et al. 2003). RAMS–ICLAMS is particularly suitable for high-resolution simulations of clouds and precipitation, as it includes a detailed two-moment (mass and number) bulk microphysical scheme (Meyers et al. 1997) describing the in-cloud processes for seven categories of hydrometeors (cloud droplets, rain droplets, pristine ice, snow, aggregates, graupel, and hail). Natural emissions (mineral dust and sea salt) are included in the model as interactive tracers for radiative transfer calculations in the GCM version of the Rapid Radiative Transfer Model (RRTMG) scheme (Mlawer et al. 1997; Iacono et al. 2000) as well as for the

TABLE 1. Storm event characteristics.

Event Date	5 Jun 2002	1 Aug 2005	15 Sep 2006
Duration (h)	22	24	34
Max event accumulated precipitation (mm)	414.5	324.9	494.4
Max hourly precipitation (mm)	194.8	87.9	73.5

TABLE 2. RAMS–ICLAMS: Model setup and characteristics.

RAMS–ICLAMS model setup	
Horizontal grid	Arakawa C grid
Horizontal resolution	24, 4, 1, and 0.25 km
Vertical grid	Sigma-z coordinates
Vertical levels	32
Convective parameterization	Kain–Fritsch (24-km grid)
Radiation parameterization	RRTMG
Initial and boundary conditions	NCEP FNL

computation of cloud condensation nuclei (CCN) and ice nuclei (IN) activation (Fountoukis and Nenes 2005; Barahona and Nenes 2009).

For the needs of this study, three distinct model domain setups were used for each storm case: 1) a two-grid setup that featured a coarse domain of 24 km with a nested 4-km grid, 2) a three-grid setup with an addition of a 1-km grid on the former setup, and 3) a four-grid setup with a nested 0.25-km grid. Convective activity on the coarser-sized grids is parameterized with the scheme of Kain and Fritsch (1993) and Kain (2004). Model extents can be seen in Fig. 1 while further details on the setup are presented in Table 2.

c. *Description and setup of the hydrologic model*

The model used to simulate the hydrologic response of the Sesia River basin is a simple spatially distributed hydrologic model [Kinematic Local Excess Model (KLEM)], which has been previously used in several flash flood studies in the same area (Sangati et al. 2009) as well as other similar mountainous regions (Borga et al. 2007; Zoccatelli et al. 2011). The distributed model is based on availability of spatially distributed information on land surface properties (topography, soil type, and land use/cover). Runoff generation within the model is based on the Soil Conservation Service curve number (SCS-CN) procedure (USDA 1986), which is applied on each grid for the spatially distributed representation of runoff generation. Following Ponce and Hawkins (1996), the value of the potential retention parameter S in the SCS-CN method for a given soil is related to the CN parameter through a calibration parameter, called infiltration storativity. The use of this parameter allows one to calibrate a spatial distribution of CN values in order to simulate correctly the observed flood water balance. A simple description of the drainage system response (Da Ros and Borga 1997) is used to represent runoff propagation, which is based on drainage paths that are distinguished between channel and hillslope paths. Differentiation between channel and hillslope grids is based on a channelization support area A_s (km^2), which is considered constant at the subbasin scale.

Discharge Q at any location along the river network is represented by

$$Q(t) = \int_A q[t - \tau(x), x]\, dx, \tag{1}$$

where A indicates the area draining to the specified outlet location, $q(t, x)$ is the runoff at time t and location x, and $\tau(x)$ is the routing time from x to the outlet of the basin specified by the region A. The routing time $\tau(x)$ is defined as

$$\tau(x) = \frac{L_h(x)}{v_h} + \frac{L_c(x)}{v_c}, \tag{2}$$

where $L_h(x)$ and $L_c(x)$ correspond to the hillslope and channel distance, respectively, which define the total flow path from point x to the watershed outlet. The velocities corresponding to hillslope v_h and channel v_h are assumed to be constant. The assumption of invariant hillslope and channel velocities has been used in a number of modeling works focused on flash floods (Giannoni et al. 2003; Nicótina et al. 2008; Marchi et al. 2010).

In summary, application of the model framework requires calibration of five parameters: the channelization support area (i.e., A_s), two kinematic parameters (v_h and v_c), the parameter of infiltration storativity used in the SCS-CN procedure, and the parameter required for the specification of the initial abstraction I_a. Given that Sangati et al. (2009) have already implemented the same modeling framework for the same study area and storms examined in this work, we used their work as reference for the values of model parameters and avoided an extensive calibration procedure.

The focus of our work is to use a hydrological model that is proven capable of representing hydrologic response for the basin and events under study in order to investigate the sensitivity of flood response for the different atmospheric simulation scenarios examined. Hydrologic analysis of the events examined in this study is not part of the scope of this work and in fact has already been carried out in the past work of Sangati et al. (2009). However, to demonstrate that the choice of model and parameters provide a realistic representation of the flood response in the area, we provide an example of observed and simulated hydrographs at the outlet of Sesia River closed at Palestro, which corresponds to the basin of interest in this study. Results are shown for the event of 2002 for which discharge observations were available. Model simulations were carried out based on observed rainfall forcing (i.e., radar rainfall), and simulated and observed flood hydrographs were compared

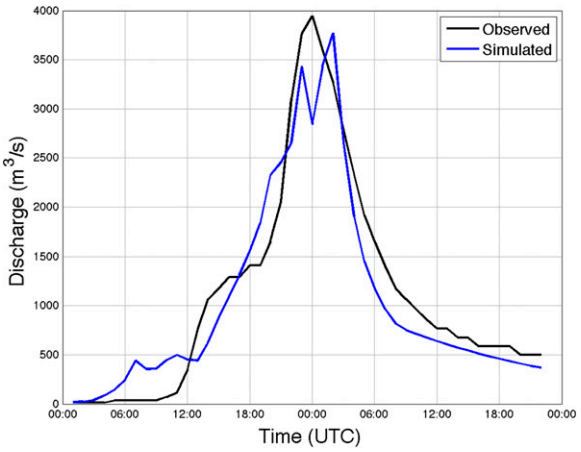

FIG. 2. Observed (black) and simulated (blue) hydrograph at the outlet of Sesia River at Palestro. Simulated hydrograph was based on radar rainfall input.

to provide an indication of the ability of the model to represent flood response at the outlet of the study basin. As is shown in Fig. 2, a simulated hydrograph captures the overall shape of a flood hydrograph (Nash–Sutcliffe score is equal to 0.9) very well and underestimates flood peak by approximately 4%. Although this level of accuracy may not fully represent other flood events, these results nonetheless provide an adequate level of confidence that the model can realistically represent rainfall-to-runoff transformation, thus allowing us to investigate the hydrologic impact of uncertainty in simulated rainfall.

d. Data used

Surface morphology plays a crucial role in the development and evolution of cloud systems. The effects of blocking on orographic precipitation have especially been thoroughly described in a number of studies (e.g., Katzfey 1995a,b; Sinclair et al. 1997; Rotunno and Ferretti 2001; Jiang 2003; Medina and Houze 2003). In this context, a high-resolution topographic dataset (3 arc s, ~90 m) from the NASA SRTM (Farr et al. 2007; Reuter et al. 2007) was used to substitute the default GTOPO30 DEM (30 arc s, ~900 m) in the atmospheric model. This implementation benefited the simulations through a more accurate slope representation as well as the estimations of local fluxes in these highly localized events. In a series of tests, the finer DEM was found to have an impact even on the 1-km-scale simulations, as a result of the model topography processor being able to derive the elevation of each grid point from a broader amount of neighboring DEM points compared to the coarser topographic dataset of 900 m. Initial and boundary conditions were provided by the NCEP Final (FNL) analyses that assimilate a vast amount of observational data through the Global Data Assimilation System (GDAS; NOAA/NCEP 2000). For the application of a hydrologic model, a higher-resolution dataset for the description of land surface was required. A DEM and CN map at 50 m resolution, derived from a regional database (M. Borga, University of Padova, 2015, personal communication), was used for hydrologic model setup.

The role of the reference dataset to serve as the ''ground truth'' was assigned to radar rainfall estimates from the Bric della Croce Doppler weather radar. The radar operates at C-band frequency and is located approximately 70 km from the study basin. Estimated rainfall fields, available at 1 km/10 min resolution were derived from radar reflectivity observations after applying a number of correction procedures (for ground clutter, atmospheric attenuation, etc.), described in detail in Sangati et al. (2009).

3. Methodology

The sensitivity of model resolution toward convection and precipitation is examined through three different model setups for a total of nine atmospheric simulations, followed by the corresponding nine basin flood response simulations. Foremost, the model setup with an inner domain of 4 km exhibits the level of detail that can be expected from a ''low maintenance'' setup in terms of computational demands. A setup with an inner grid of 1 km represents a scale with cloud-resolving capability, whereas the addition of a very fine grid (0.25 km) investigates the potential benefits from the presence of a subkilometer grid.

For each model setup, distinct model simulations took place to provide rainfall datasets for each scale that stand unaffected by the existence of finer grids via the two-way nesting in the model. This is a key element that differentiates this comparison from a plain juxtaposition of different domain outputs from a single simulation. The datasets were reprojected and brought to the same scale as the reference dataset (in our case, the radar rainfall estimates) in order for the common-scale comparison to take place.

The results are presented in various forms, the first of which is rainfall accumulation maps that serve as a primal overview of the model accordance versus radar estimates. A qualitative analysis that includes vertical cross sections of the cloud structure in times of maximum rainfall activity, and focusing in cloud composition characteristics (ice, liquid, and graupel mixing ratios), is done to provide insight on the nature and unique characteristics.

In quantitative terms, quantile–quantile (Q–Q) plots from the model and radar hourly estimates are used to assess the accuracy of simulated rainfall fields to capture the observed rainfall distribution (5%–95%). Additional statistical information is provided via Taylor diagrams (Taylor 2001), which concentrate the correlation coefficient (COR), the root-mean-square difference (RMSD), and the standard deviation (STD) of the model and radar estimates in a single plot, evaluating the agreement in terms of spatial distribution. As the mountainous areas within the model domain constitute hotspots where benefits of a finer grid are more likely to manifest, a second set of statistics is presented, conditioned to higher-altitude areas ($\geq$1000 m). In addition to the point-by-point comparison of the various datasets, a further analysis on a neighborhood approach basis (Roberts and Lean 2008; Schwartz et al. 2009) is presented in terms of fraction skill scores (FSSs) for a number of different radii and rainfall threshold values. Finally, evaluation in terms of flood response is carried out by comparing simulated runoff at Sesia River basin (Fig. 1) with corresponding reference (i.e., radar rainfall)-based simulations. Error metrics [root-mean-square error (RMSE) and relative error] and correlation values are calculated and presented for different hydrograph properties (e.g., runoff volume and peak).

4. Analysis and results

The three selected cases consist of two deep convective precipitation events (2002 and 2005), which are typical in Alpine high-elevation mountainous areas, and a long-lasting stratiform event in 2006. Hence, the responses of NWP and hydrological simulations are showcased in diverse conditions. The main synoptic aspects of each event are described below, followed by the analyses of the statistical scores, both for the atmospheric and the hydrological parts.

a. Meteorological analysis

The establishment of a low pressure system over western Europe on 4 June 2002 favored the transport of moist air from the Mediterranean Sea toward the Alps. Orographic triggering of convection resulted in a severe flood event over the Sesia River basin. A vertical cross section (Fig. 3b) from the 0.25-km domain at the time and location of maximum precipitation rate indicates the development of a seeder–feeder mechanism. The deep convective cloud (seeder) extends up to 12 km and effectively supplies the lower mixed-phase cloud (feeder) with ice, therefore increasing the precipitation amounts on the surface. The ice mixing ratio values at this specific hour reached 3.261 g kg^{-1} (Fig. 3b). Updrafts up to 18.39 m s^{-1} that are evident in the core of the cloud (Fig. 3c) clearly support the assertions on the deep convective nature of the event. A further microphysical analysis shows significant amounts of supercooled liquid droplets that are transferred along the intense updraft toward the upper layers of the cloud at temperatures below 0°C (Fig. 3d). The release of latent heat at these heights due to the freezing of the supercooled droplets provides an additional mechanism that invigorates convection. Availability of liquid water in the middle and upper parts of the cloud leads to the formation of graupel and hail (Fig. 3e), the riming and melting of which contributes to the high rainfall rates.

In terms of dynamical forcing, the 2005 storm featured a quite similar structure, its distinction being a comparatively lower rainfall magnitude, both in total (325 vs 414 mm) and hourly accumulation values (88 vs 195 mm). This episode was a result of the sequential passing of two convective storms within the same day and, compared to 2002, affected a limited extent of the hydrological basin, focused mainly toward the northwestern part. The 2006 event spanned within 48 h of near-continuous rainfall from a stratiform system that was blocked from the northern high mountain barrier of the Monte Rosa massif. A vertical cross section during an hour of intense rainfall rate displays the difference of this storm with the previous two events and verifies the stratiform nature from the confined extent of the cloud structure as well as liquid water content values that in comparison stand lower, reaching maximum values of 1.24 g kg^{-1} (Fig. 4).

b. NWP error analysis

1) THE CASE OF JUNE 2002

The overview of the radar estimates alongside the three model grid setups (0.25, 1, and 4 km) are displayed in Fig. 5. Beginning at 1000 UTC 4 June 2002 and onward, the Doppler radar recorded rainfall accumulations of 414 mm within 35 h. Over the mountainous part of the domain, the 0.25-km simulation presented a mere average underestimation of 4%. The maximum accumulation domainwide was 431 mm, with the main improvement being the rainfall distribution over the basin. The 0.25-km simulation presented a significantly better positioning of the rainfall core among the three datasets when compared to the radar. The domainwide comparison for 2002 comes down to a small underestimation from the model in all three grid spacing setups, with estimates from finer grids being in better agreement with the radar (Fig. 6a). When focusing on higher-elevation areas of northwestern Italy, the benefits of the higher resolution become more obvious, with differences between

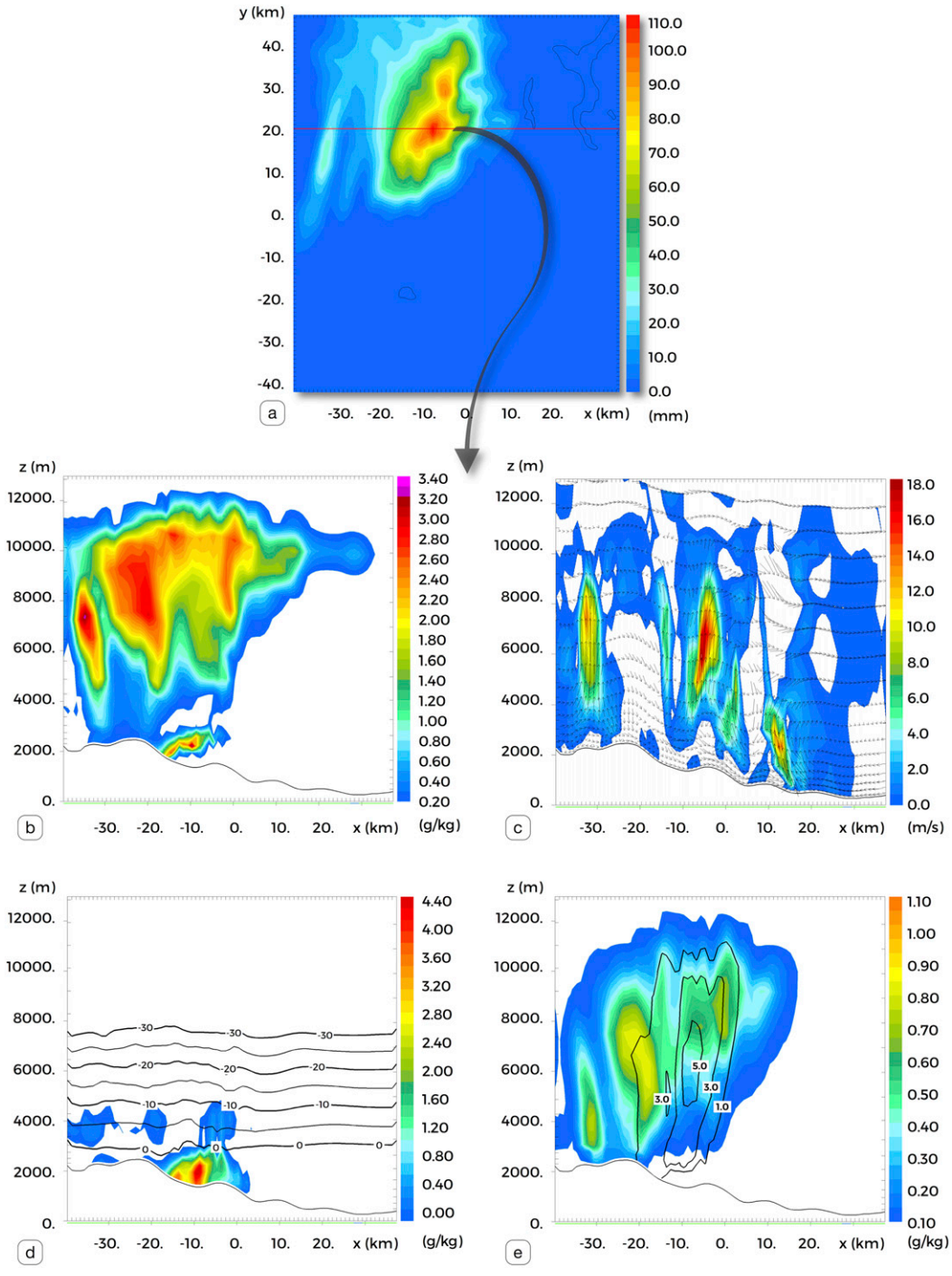

FIG. 3. (a) Accumulated precipitation (mm) during an hour of intense rainfall activity in 2002. Vertical cross sections (east–west) along the red line are presented for the following parameters: (b) ice mixing ratio (g kg^{-1}), (c) vertical wind speed and direction (m s^{-1}), (d) liquid mixing ratio (g kg^{-1}) and temperature (°C), and (e) graupel (shaded) and hail (contoured) mixing ratios (g kg^{-1}).

the three model datasets becoming quite notable in the Q–Q plots. The 0.25-km simulation clearly outperforms the rest, showcasing a quite satisfactory overall agreement with the radar and a nearly identical image for accumulation values within the 0–25 mm h^{-1} range (Fig. 6b). The beneficial role of higher resolution becomes more evident in the Taylor diagrams (Figs. 7a,b) and FSS plots (Fig. 8). The COR of the 0.25-km dataset

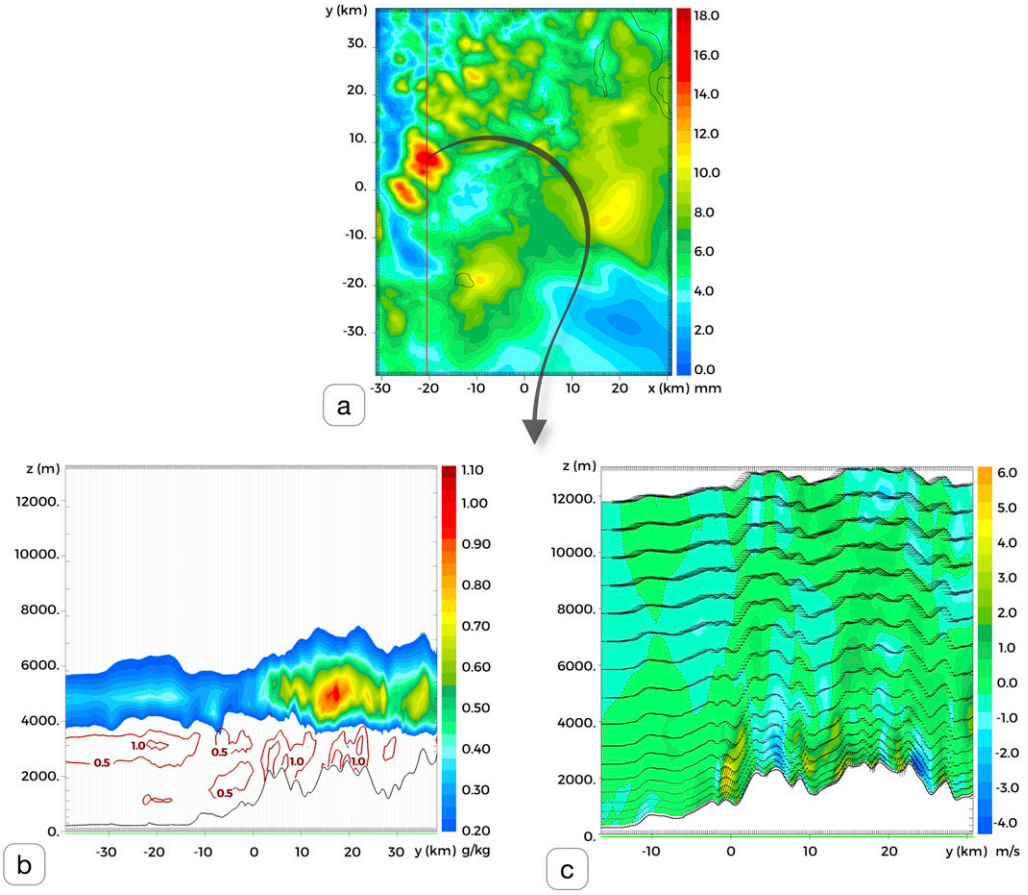

FIG. 4. (a) Accumulated precipitation (mm) during an hour of intense rainfall activity in 2006. Vertical cross sections (north–south) along the red line are presented for the following parameters: (b) ice mixing ratio (g kg^{-1}) and (c) vertical wind speed (m s^{-1}) and direction.

in mountainous areas is 0.75, whereas 1 and 4 km stand at 0.31 and 0.39, respectively (Fig. 7b). In the FSS plots, the 0.25-km simulation stands apart, showcasing very good behavior, especially toward high rainfall thresholds (exceeding 100 and 250 mm). Better accuracy at this end of the rainfall spectrum is obviously of utmost importance in terms of flash flood response. With a broad neighborhood radii value, the FSSs are 0.80, 0.69, and 0.54 for the 0.25-, 1-, and 4-km simulations, respectively, whereas under a tighter neighborhood radii value the scores drop to 0.65, 0.45, and 0.25, respectively. The notable distinction between the three model datasets becomes obvious for total rainfall values that exceed 50 mm (Figs. 8a–d).

2) THE CASE OF AUGUST 2005

The 2005 event featured lower rainfall accumulation values in comparison. The rain gauge calibrated radar recorded peak accumulations of 325 mm over a period of 23 h (from 1900 UTC 1 August to 1800 UTC 2 August). The model successfully estimated the spatial rainfall pattern but underestimated the overall basin-average quantity in all three model setups. The maximum total accumulations were 164 mm in the 1-km simulation and 197 mm in the 0.25-km simulation. Once again, the higher-resolution simulation featured a considerably better placement of the peak accumulation area toward the southwest of the mountainous range, in very good agreement with the radar. The arrangement of the model datasets in the Q–Q plot of the 2005 episode is such that consensus with the radar gets better as grid spacings get finer (Figs. 6c,d). Underestimation is evident both in the domainwide analysis and the conditioned Q–Q comparison. The differences between the 0.25- and 1-km datasets in the domainwide analysis (Fig. 6c) are further distinguished on the conditioned statistical set (Fig. 6d), where 0.25 km clearly stands out. While a slight improvement in the estimated rainfall between 1 and 0.25 km magnitude is notable, the significant role of the finer grid in that specific case lies in the spatial distribution

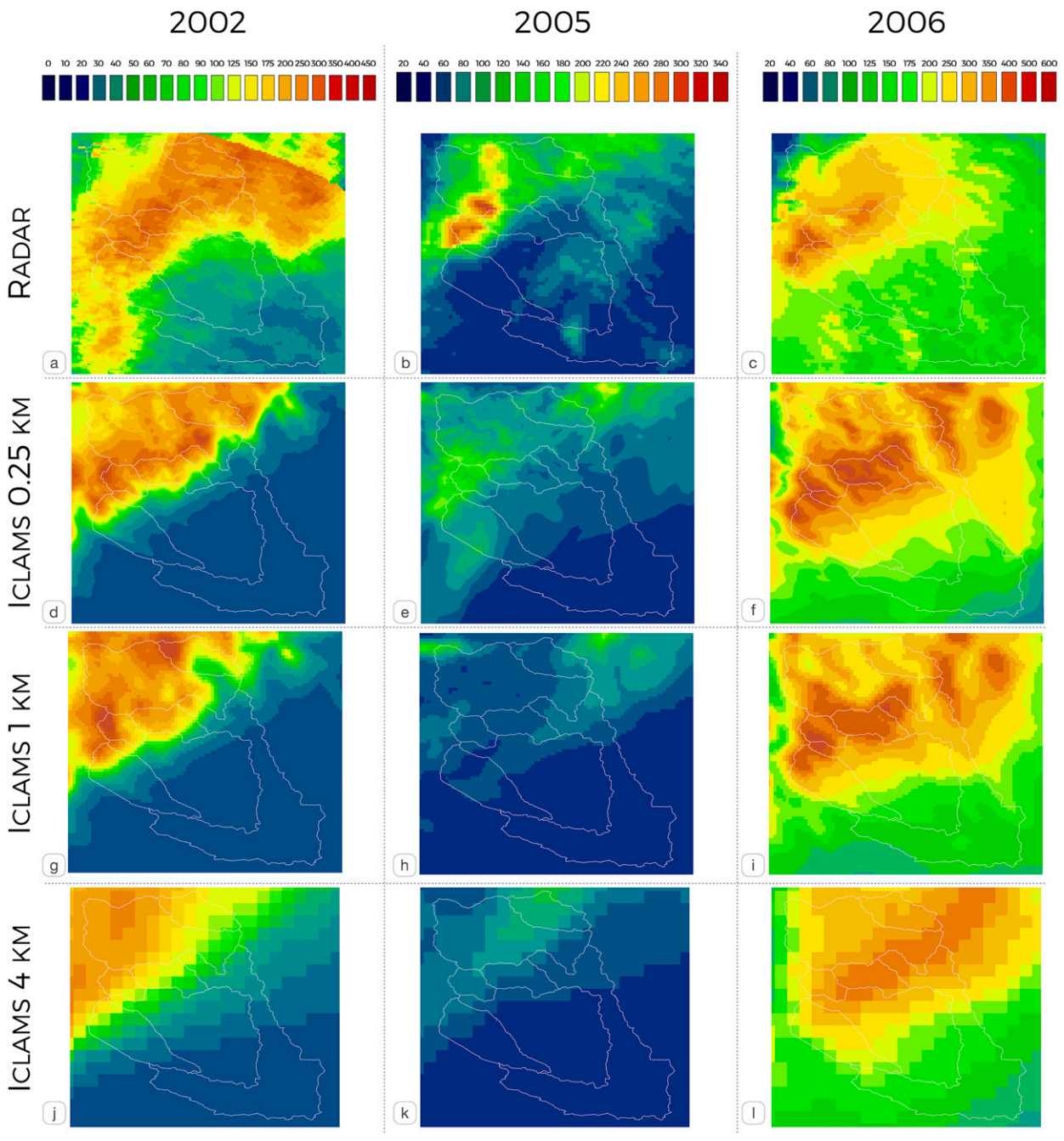

FIG. 5. Accumulated precipitation (mm) comparison between (a)–(c) the radar rainfall estimates and (d)–(l) the RAMS–ICLAMS simulations of the three storm events from different model grid scale setups.

of rainfall. The improved variability and pattern of rainfall from the 0.25-km simulation are supported by the STD and COR scores in the Taylor diagrams (Figs. 7c,d). The FSS plots clearly support the better agreement of the 0.25-km simulation with the radar (Figs. 8e–h). As this was a highly localized event with rainfall accumulations being confined to the northwestern high mountain area, the application of the method with a broad radius (Fig. 8h) resulted in lower scores compared to the tighter radii of 2, 5, and 10 km (Figs. 8e–g).

3) THE CASE OF SEPTEMBER 2006

The flooding event of September 2006 was quite contrasting to the aforementioned two events. It was a result of a synoptic system that was stationary over the basin area, persisted for a period of nearly 2 days, and featured

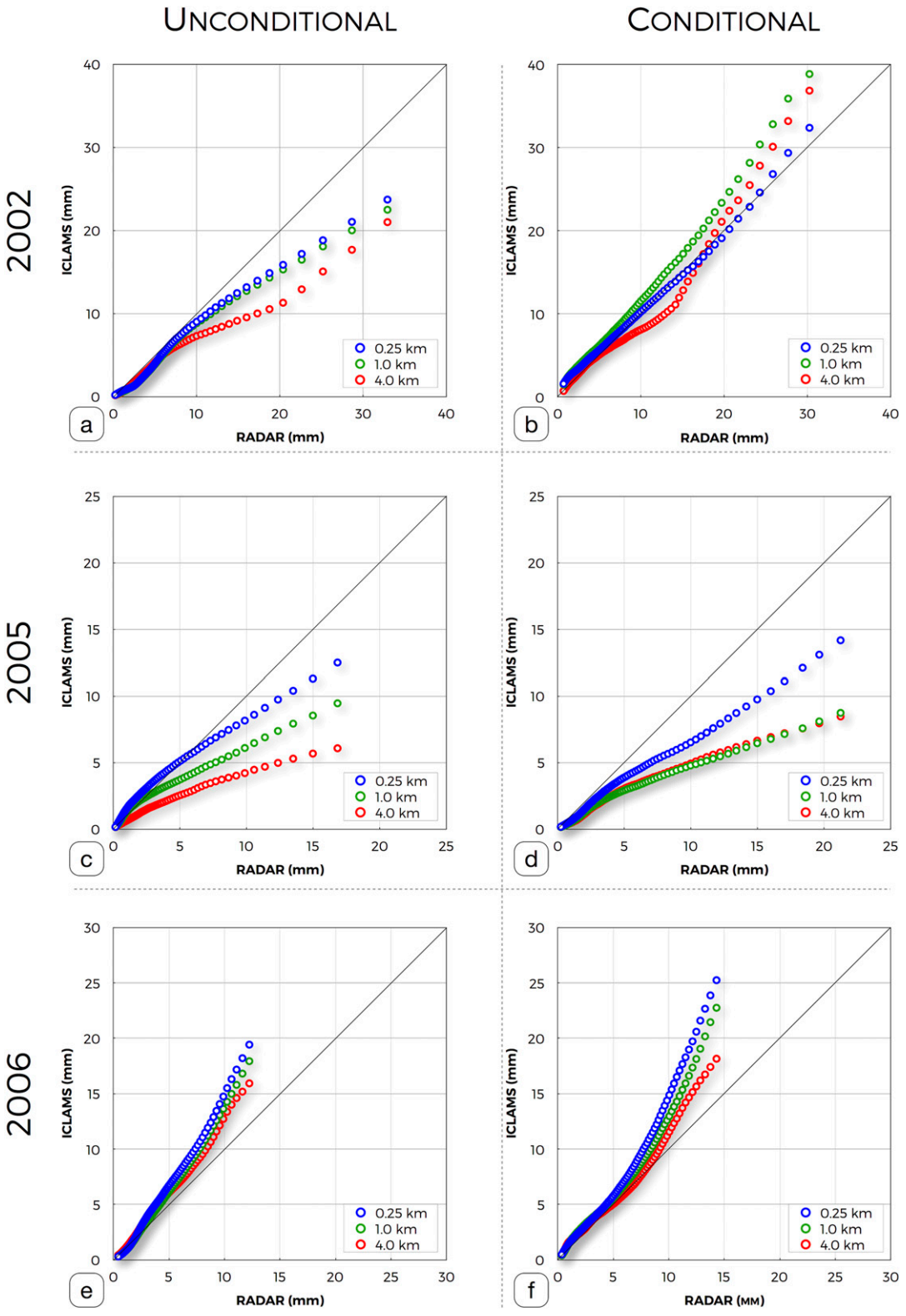

FIG. 6. Q–Q plots (RAMS–ICLAMS setups vs radar). Unconditional statistics are calculated domainwide, whereas conditional statistics are focused solely on mountainous terrain (≥1000 m).

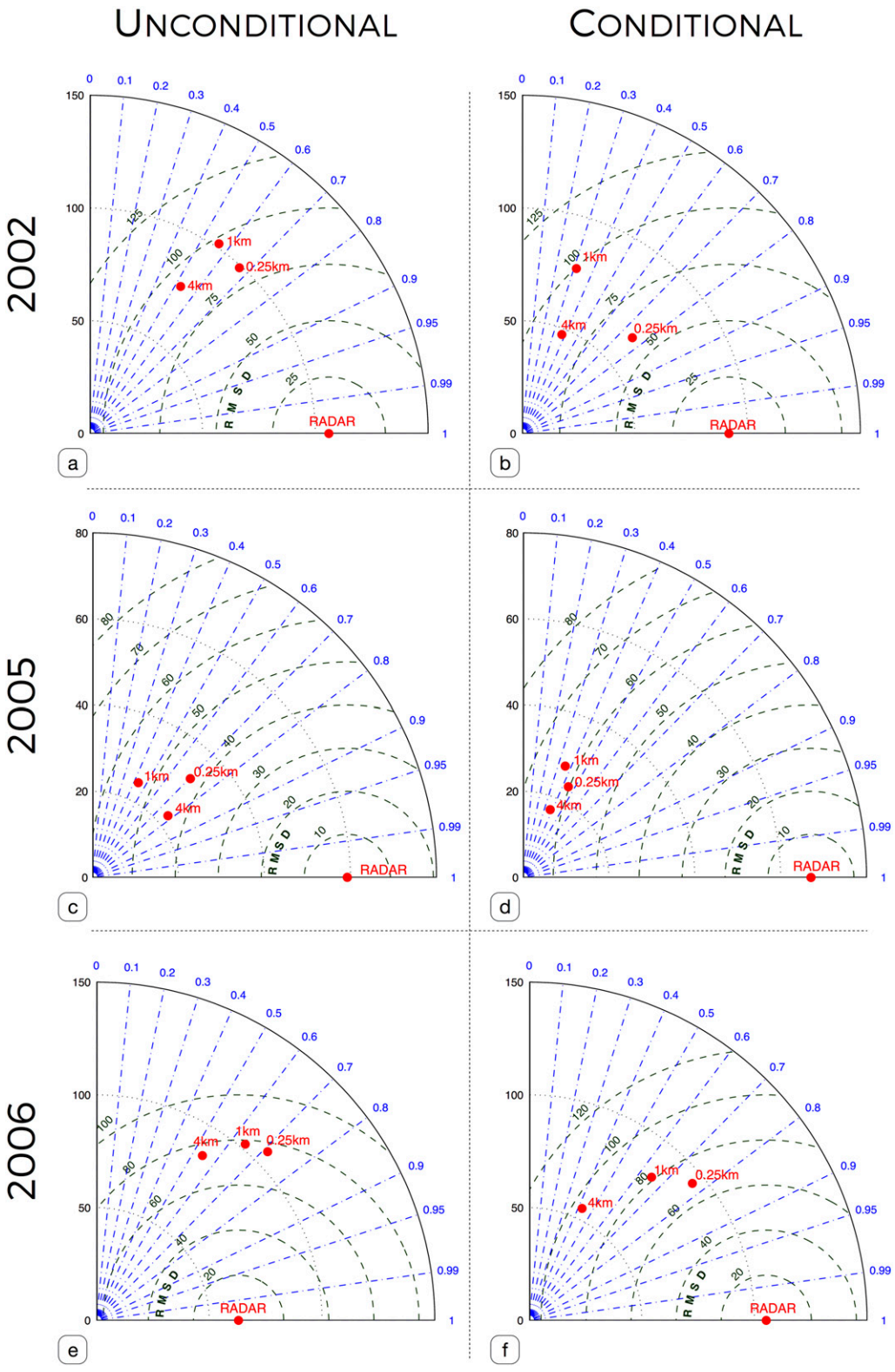

FIG. 7. Taylor diagrams for all datasets (radar and RAMS–ICLAMS simulations).

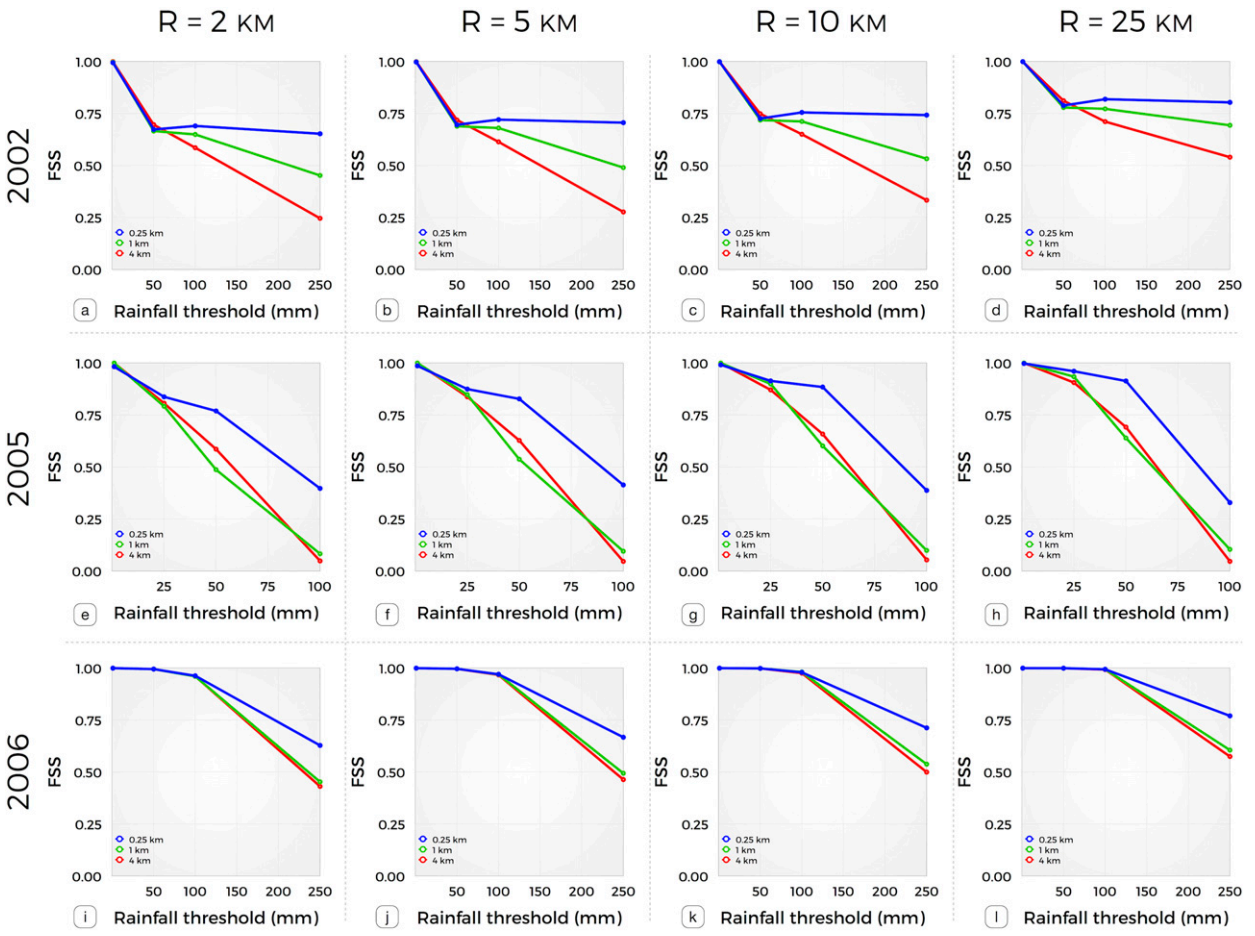

FIG. 8. FSS scores of the RAMS–ICLAMS simulations for a number of total rainfall thresholds and radii.

lower hourly accumulation values in comparison (74 vs 195 mm in 2002; Table 1). The positioning of rainfall stands in quite satisfying agreement, but the magnitude is clearly overestimated by both the 1- and 0.25-km setups. This is the only event where overestimation in the rainfall amounts is evident, regardless of the grid resolution. The cross sections in Figs. 4b and 4c reveal the confinement of ice particles within altitudes of 4–7 km and water vapor mixing ratio values a little above 1.0 g kg^{-1}. The updrafts remained much weaker compared to the deep convective events, reaching maximum values of 7 m s^{-1}. In terms of rainfall magnitude, the 4-km setup seemingly outperforms the finer grids and presents the best agreement with the radar (Figs. 6e,f), which at first appears as an oxymoron. However, the decreased susceptibility of the coarser grid toward convection partly counterbalanced the overestimation of the finer grids and showcased good results for the wrong reason. The rest of the statistical analysis favors the results of the finest grid. The Taylor diagrams suggest better granularity in the spatial pattern of rainfall from the 0.25-km simulation (Figs. 7e,f) as well as present better COR scores (0.71 for the 0.25-km simulation, as opposed to 0.55 for 4 km). The FSS plots for that case (Figs. 8i–l) once again present higher scores for the 0.25-km simulation compared to the coarser datasets (0.77, 0.61, and 0.57 for the 0.25-, 1-, and 4-km simulations, respectively). See section 4d for further discussion on this interesting case.

c. *Hydrologic error analysis*

In this section, the hydrological impact of the different rainfall simulation scenarios is examined to highlight the benefits and limitations of using rainfall forcing from atmospheric simulations for modeling flash flood response. Simulated rainfall for the different model resolutions (0.25, 1, and 4 km) is used to force the hydrologic model, and results are compared against the reference (i.e., radar rainfall)-based simulations. Simulated hydrographs and corresponding hyetographs for all forcing scenarios (simulated and reference) are presented in Fig. 9 for all three storms examined.

In this case, the reference spatial domain for the analysis corresponds to the area of the Sesia River basin

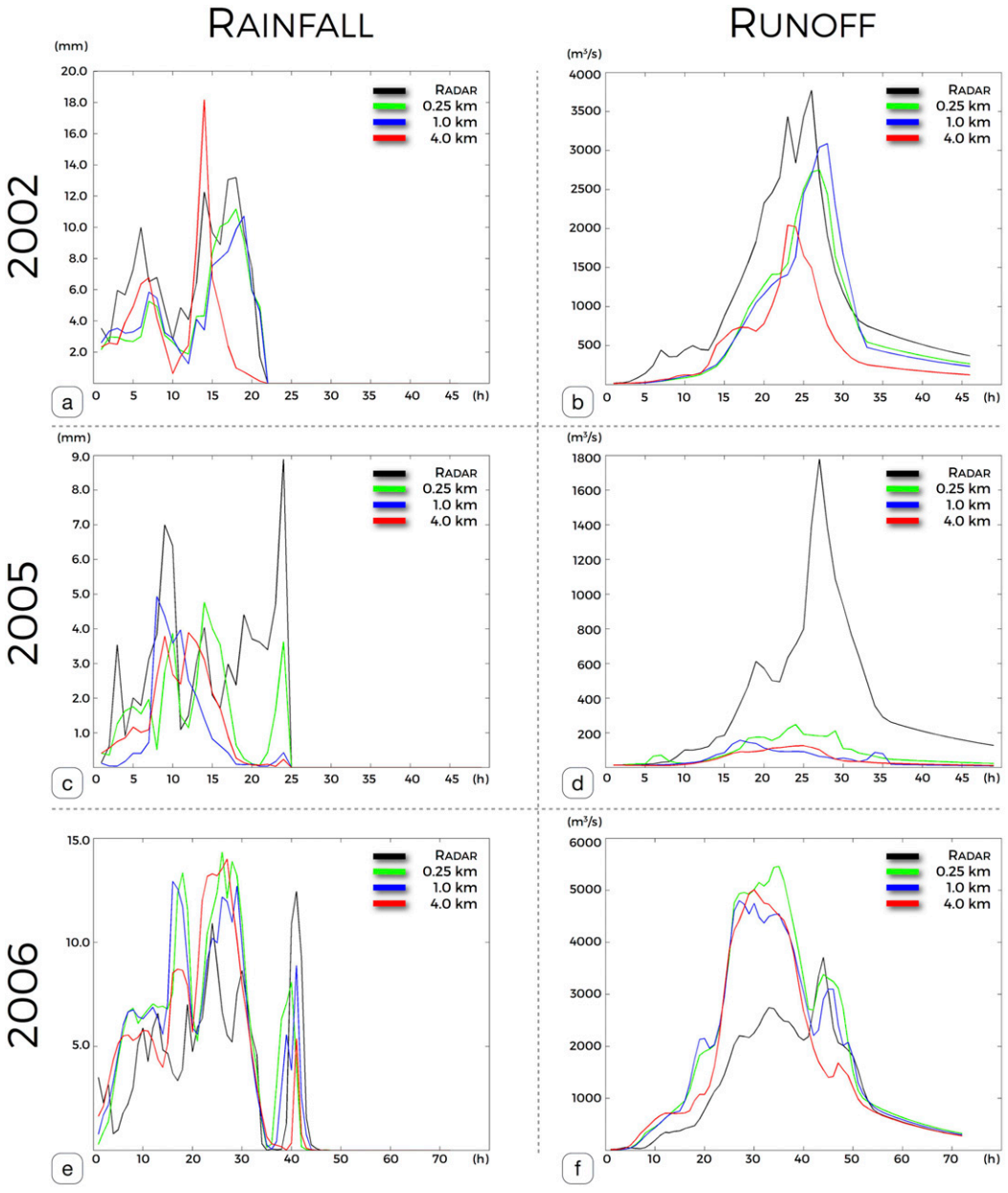

FIG. 9. Rainfall (mm h^{-1}) and corresponding runoff ($m^3 s^{-1}$) time series for the (a),(b) 2002; (c),(d) 2005; and (e),(f) 2006 events.

(Fig. 1). Visual examination of the temporal evolution of basin-average rainfall (Fig. 9) for the different rainfall scenarios reveals that simulated rainfall follows well the temporal dynamics of reference rainfall in almost all cases. This is also quantitatively supported based on the correlation coefficient between simulated and reference basin-average rainfall (Table 3). Apart from the case of 2005, where correlation for 1- and 4-km simulations was relatively low (0.5), the rest of cases have correlation values ≥0.7, with the highest values being associated with 0.25- and 1-km resolutions. Superiority of the highest-resolution scenarios (relative to the lowest resolution) is also apparent for other error metrics examined, namely, the RMSE and relative error (Table 3). However, despite the high degree of correlation between reference and simulated rainfall, considerable discrepancies in total basin-average rainfall exist. The significance of these discrepancies varies with simulation scenario (i.e., model resolution) and storm event. It is noted that for the two convective-type events (2002 and

TABLE 3. Comparison of basin-average rainfall and simulated runoff between reference forcing and ICLAMS simulations at different resolutions. Summary statistics are shown for the three events (2002, 2005, and 2006) and include Pearson's correlation coefficient (COR), RMSE, and relative error.

	Basin-avg rainfall			Runoff			Peak runoff
ICLAMS	COR	RMSE (mm)	Relative error (%)	COR	RMSE (mm)	Relative error (%)	Relative error (%)
2002							
0.25 km	0.9	2.1	−28.6	0.9	536	−31.5	−27.0
1 km	0.9	2.2	−29.9	0.8	629	−30.7	−18.1
4 km	0.7	3.4	−42.9	0.9	784	−55.8	−45.8
2005							
0.25 km	0.7	1.7	−45.1	0.8	449	−78.2	−86.1
1 km	0.5	2.1	−64.2	0.4	496	−87.0	−91.2
4 km	0.5	2.1	−56.3	0.7	493	−88.2	−93.0
2006							
0.25 km	0.7	3.3	39.5	0.9	1245	63.7	47.1
1 km	0.8	2.9	31.5	0.9	1057	51.1	29.4
4 km	0.7	3.0	21.6	0.8	1096	35.4	35.0

2005 cases), all model scenarios consistently underestimated basin-average rainfall by 30%–40% for 2002 and by 45%–64% for 2005 (Table 3), while in the stratiform case of 2006 they all consistently overestimated rainfall by approximately 20%–40%.

The impact of rainfall differences on simulating flood response is analyzed by comparing the simulated hydrographs based on model and reference rainfall input (Fig. 9). Examination of each event reveals a number of interesting and contrasting outcomes regarding the benefit of using high-resolution atmospheric simulations for flash flood prediction. The most severe event of 2002 constitutes the best case in demonstrating that by using simulated rainfall at high resolution, we could adequately capture the magnitude and overall shape of the reference flash flood hydrograph. An underestimation of total runoff on the order of ~30% is consistent with the bias in rainfall input (Table 3) for the higher-resolution scenarios (0.25 and 1 km), while for the 4-km resolution, a magnification in relative error in total runoff is observed. Interestingly, despite the fact that error metrics for both rainfall and runoff are very similar between 0.25- and 1-km resolution scenarios, the difference in simulated peak flow is apparent and highlights its sensitivity to spatial rainfall distribution differences (Figs. 9a,b).

In the case of 2005, high-resolution scenarios performed marginally better in comparison to coarse resolution, but underestimation in all cases was so severe that there was not even a clear flood hydrograph signature shown in the corresponding simulations (Figs. 9c,d). This is a clear indication that high model resolution is not the only important factor for accurately capturing highly localized severe convective events. In contrast with the underestimation of the first two events, the case of 2006 exhibited considerable overestimation of runoff with relative error ranging from 35% to 64% in total runoff and from 29% to 47% in peak runoff. Apart from the contrast in the direction of the error in this case, there is a counterintuitive outcome on the ranking of performance with respect to resolution, which leaves as least performing the highest-resolution scenario, while the 1- or 4-km scenarios are the best performing, depending on the metric used. Examining the temporal evolution of rainfall and runoff (Figs. 9e,f) for this case, it is apparent that the overestimation is due to the strong overestimation of the first part of the rainfall event, while the second rainfall peak, which according to the reference was the one responsible for the flow peak, is underestimated.

Overall, propagation of rainfall error to runoff error, estimated as the ratio of relative error in runoff over relative error in rainfall, is greater than one in all cases, and it varies considerably with scale (e.g., 1.1–1.7 for 0.25-km scenario) or with storm event (e.g., 1.3–1.7 for 2005), demonstrating the magnification of error propagation from rainfall to runoff and its nonlinear dependence on rainfall characteristics. This relates to the fact that differences in hydrologic response at the outlet of the basin are not only a result of differences in rainfall volume, but are also attributed to differences in the spatial pattern of rainfall (Fig. 5) over the basin and initial soil moisture conditions (Sangati and Borga 2009; Nikolopoulos et al. 2011).

d. Discussion

Three heavy precipitation events that induced extreme flash floods with diverse characteristics in terms of dynamical forcing as well as rainfall duration and magnitude were examined in terms of atmospheric and hydrologic simulations. Overall, the employment of a very

fine (0.25 km) grid seemed to benefit the atmospheric model simulations. It contributed toward a more detailed reproduction of the convection processes explicitly, as a result of a greater number of grid points falling within the cloud structure. Despite convective precipitation positioning being a common drawback of NWP, especially over mountainous terrain (Weckwerth and Parsons 2006), this was not the case in any of the three simulations that are presented in this study.

Among the three selected cases, the best agreement with the reference dataset was evident in the deep convective event of 2002, where benefits from a very fine resolution grid were notable both in terms of rainfall quantity and spatial distribution. The comparison of the rainfall estimates for the 2005 storm underlined that in cases where the model estimation was not in good agreement with the radar, the addition of a higher-resolution grid did not rectify all of the things that were wrong. However, even in this far-from-ideal case, apparent benefits in the distribution of rainfall were notable.

In the long-lasting stratiform event of 2006, where overestimation characterized the output from all model setups, statistics once more indicated better correlation and lower error scores to the estimates of the 0.25-km grid. For this specific incident, a concern on the range effect of the radar estimates comes to surface. The point obviously is not to question the integrity of the reference dataset. However, radar rainfall estimates feature an inherent tendency toward underestimation of stratiform precipitation, especially in ranges beyond the melting layer (Hazenberg et al. 2011). Numerous techniques have been developed to correct for this vertical reflectivity profile effect (Kitchen and Jackson 1993; Joss and Lee 1995; Ciach et al. 1997; Anagnostou and Krajewski 1999; Pellarin et al. 2002; Gourley et al. 2009; Delrieu et al. 2009). In our case, the radar estimates were already corrected for that matter, so this drawback is probably cured in the final dataset. Nevertheless, the very good level of agreement between the model and the radar in terms of spatial distribution triggered a suspicion that the disagreement on rainfall magnitude might be partially accustomed to this specific limitation. The high altitude of the headwaters of the study basin, where fewer rain gauges are presumably located, could raise a hypothesis on the excess precipitation amounts of the model compared to radar having occurred in a solid form (snow). However such a speculation demands a careful evaluation regarding the existence of snow, which was not available.

Evaluation of the impact of atmospheric model resolution on simulating flood response proved to be a highly penalizing process because of magnification of error from rainfall to runoff. Except for the 2002 event, where results demonstrate clearly that the use of a high-resolution setup (0.25 or 1 km) leads to considerable improvement in capturing flash flood response, the other two cases showed that bias in rainfall was notable in all resolutions that had severe impact on flood simulations. As stated above, this indicates that while higher resolution can be a necessary step for advancing flash flood forecasting, it is certainly not the only factor responsible for achieving accurate quantitative precipitation and flood forecasts.

5. Conclusions

In this paper, our goal was to examine the impact of fine atmospheric model grid spacing on the simulations of mountainous flash flood–inducing heavy precipitation events and to investigate the corresponding effect on the simulations of hydrological response.

The presented results exhibit the beneficial role of finer grid scales, especially toward more accurate rainfall distribution fields. Nevertheless, it becomes apparent that model resolution neither is, nor should be, treated as a universal remedy on which to rely for the addressing of all limitations of flash flood forecasting. A gainful impact was evident from the statistical analysis both in terms of rainfall magnitude as well as the granularity of the precipitation variability. Yet, deviation between model and radar estimations was evident in both directions (underestimation for the convective event of 2005 and overestimation of the stratiform event of 2006). Moving toward finer scales constitutes a step in the right direction, but it is not the sole component of a successful flash flood–forecasting recipe.

The different nature of the selected events, as well as the separation of the statistical analysis in mountainous and domainwide applications, provided a better perception of the characteristics that can be applied in similar NWP applications in other complex terrain areas.

Hydrologic evaluation followed the general pattern of findings demonstrating a case (2002 event) where high-resolution simulations resulted in significant improvement, while for the other two events, deviation from reference hydrographs was severe and thus the marginal improvement due to resolution did not affect the accuracy of the simulations. The nonlinear error propagation from rainfall to runoff showed clearly that differentiation in rainfall magnitude and pattern can magnify considerably when translating to runoff, which further highlights the complexities and challenges involved in flash flood forecasting.

Future plans are bound to the delimitation of the forecasting uncertainty and include a set of sensitivity tests on the susceptibility of orographic convection

toward aerosol forcing. With deep convective events over mountainous areas being dominated by ice processes, the improved representation in the model through prognostic treatment of airborne particles (dust and salt) as CCN and IN is expected to provide an important insight on the aerosol–cloud–precipitation interactions and their respectful impact on rainfall predictions (Solomos et al. 2011).

Finally, a number of simulations in various data-rich mountainous regions are needed to broaden the validation of NWP estimates, further circumscribe their common characteristics, and examine novel uses such as the satellite correction procedures described in Zhang et al. (2013) and Nikolopoulos et al. (2015).

Acknowledgments. The authors wish to express their gratitude to Prof. Marco Borga and Dr. Davide Zoccatelli (University of Padova) for making available all the necessary data (radar rainfall, regional land surface maps, and discharge data) for this study. We would also like to thank the two anonymous reviewers for their constructive comments that helped us improve this manuscript. This research was supported by the FP7 project eartH2Observe (Grant Agreement 603608).

REFERENCES

Anagnostou, E. N., and W. F. Krajewski, 1999: Real-time radar rainfall estimation. Part I: Algorithm formulation. *J. Atmos. Oceanic Technol.*, **16**, 189–197, doi:10.1175/1520-0426(1999)016<0189:RTRREP>2.0.CO;2.

Barahona, D., and A. Nenes, 2009: Parameterizing the competition between homogeneous and heterogeneous freezing in ice cloud formation—Polydisperse ice nuclei. *Atmos. Chem. Phys.*, **9**, 5933–5948, doi:10.5194/acp-9-5933-2009.

Bernardet, L. R., L. D. Grasso, J. E. Nachamkin, C. A. Finley, and W. R. Cotton, 2000: Simulating convective events using a high-resolution mesoscale model. *J. Geophys. Res.*, **105**, 14 963–14 982, doi:10.1029/2000JD900100.

Borga, M., P. Boscolo, F. Zanon, and M. Sangati, 2007: Hydrometeorological analysis of the 29 August 2003 flash flood in the eastern Italian Alps. *J. Hydrometeor.*, **8**, 1049–1067, doi:10.1175/JHM593.1.

Bougeault, P., and Coauthors, 2001: The MAP Special Observing Period. *Bull. Amer. Meteor. Soc.*, **82**, 433–462, doi:10.1175/1520-0477(2001)082<0433:TMSOP>2.3.CO;2.

Bouilloud, L., G. Delrieu, B. Boudevillain, and P. E. Kirstetter, 2010: Radar rainfall estimation in the context of post-event analysis of flash flood events. *J. Hydrol.*, **394**, 17–27, doi:10.1016/j.jhydrol.2010.02.035.

Buzzi, A., S. Davolio, P. Malguzzi, O. Drofa, and D. Mastrangelo, 2014: Heavy rainfall episodes over Liguria in autumn 2011: Numerical forecasting experiments. *Nat. Hazards Earth Syst. Sci.*, **14**, 1325–1340, doi:10.5194/nhess-14-1325-2014.

Ciach, G. J., W. F. Krajewski, E. N. Anagnostou, M. L. Baeck, J. A. Smith, J. R. McCollum, and A. Kruger, 1997: Radar rainfall estimation for ground validation studies of the Tropical Rainfall Measuring Mission. *J. Appl. Meteor.*, **36**, 735–747, doi:10.1175/1520-0450-36.6.735.

Colle, B. A., and C. F. Mass, 2000: The 5–9 February 1996 flooding event over the Pacific Northwest: Sensitivity studies and evaluation of the MM5 precipitation forecasts. *Mon. Wea. Rev.*, **128**, 593–617, doi:10.1175/1520-0493(2000)128<0593:TFFEOT>2.0.CO;2.

——, J. B. Wolfe, W. J. Steenburgh, D. E. Kingsmill, J. A. W. Cox, and J. C. Shafer, 2005: High-resolution simulations and microphysical validation of an orographic precipitation event over the Wasatch Mountains during IPEX IOP3. *Mon. Wea. Rev.*, **133**, 2947–2971, doi:10.1175/MWR3017.1.

Cotton, W. R., and Coauthors, 2003: RAMS 2001: Current status and future directions. *Meteor. Atmos. Phys.*, **82**, 5–29, doi:10.1007/s00703-001-0584-9.

Da Ros, D., and M. Borga, 1997: Use of digital elevation model data for the derivation of the geomorphological instantaneous unit hydrograph. *Hydrol. Processes*, **11**, 13–33, doi:10.1002/(SICI)1099-1085(199701)11:1<13::AID-HYP400>3.0.CO;2-M.

Davolio, S., F. Silvestro, and P. Malguzzi, 2015: Effects of increasing horizontal resolution in a convection-permitting model on flood forecasting: The 2011 dramatic events in Liguria, Italy. *J. Hydrometeor.*, **16**, 1843–1856, doi:10.1175/JHM-D-14-0094.1.

Delrieu, G., B. Boudevillain, J. Nicol, B. Chapon, P. E. Kirstetter, H. Andrieu, and D. Faure, 2009: Bollène-2002 Experiment: Radar quantitative precipitation estimation in the Cévennes–Vivarais region, France. *J. Appl. Meteor. Climatol.*, **48**, 1422–1447, doi:10.1175/2008JAMC1987.1.

Doocy, S., A. Daniels, S. Murray, and T. D. Kirsch, 2013: The human impact of floods: A historical review of events 1980–2009 and systematic literature review. *PLoS Curr. Disasters*, doi:10.1371/currents.dis.f4deb457904936b07c09daa98ee8171a.

Drobinski, P., and Coauthors, 2014: HyMeX: A 10-year multidisciplinary program on the Mediterranean water cycle. *Bull. Amer. Meteor. Soc.*, **95**, 1063–1082, doi:10.1175/BAMS-D-12-00242.1.

Ducrocq, V., and Coauthors, 2014: HyMeX-SOP1: The field campaign dedicated to heavy precipitation and flash flooding in the northwestern Mediterranean. *Bull. Amer. Meteor. Soc.*, **95**, 1083–1100, doi:10.1175/BAMS-D-12-00244.1.

Farr, T. G., and Coauthors, 2007: The Shuttle Radar Topography Mission. *Rev. Geophys.*, **45**, RG2004–RG2033, doi:10.1029/2005RG000183.

Fountoukis, C., and A. Nenes, 2005: Continued development of a cloud droplet formation parameterization for global climate models. *J. Geophys. Res.*, **110**, D11212, doi:10.1029/2004JD005591.

Fritsch, J. M., and R. E. Carbone, 2004: Improving quantitative precipitation forecasts in the warm season: A USWRP research and development strategy. *Bull. Amer. Meteor. Soc.*, **85**, 955–965, doi:10.1175/BAMS-85-7-955.

Fuhrer, O., 2005: From advection to convection: Dynamical and numerical issues in high-resolution modeling of atmospheric flows past topography. Ph.D. thesis, ETH Zurich, 151 pp., doi:10.3929/ethz-a-005035587.

Giannoni, F., J. A. Smith, and G. Roth, 2003: Hydrologic modelling of extreme floods using radar rainfall estimates. *Adv. Water Resour.*, **26**, 195–203, doi:10.1016/S0309-1708(02)00091-X.

Gourley, J. J., D. P. Jorgensen, S. Y. Matrosov, and Z. L. Flamig, 2009: Evaluation of incremental improvements to quantitative precipitation estimates in complex terrain. *J. Hydrometeor.*, **10**, 1507–1520, doi:10.1175/2009JHM1125.1.

Hazenberg, P., H. Leijnse, and R. Uijlenhoet, 2011: Radar rainfall estimation of stratiform winter precipitation in the Belgian Ardennes. *Water Resour. Res.*, **47**, W02507, doi:10.1029/2010WR009068.

Iacono, M. J., E. J. Mlawer, S. A. Clough, and J.-J. Morcrette, 2000: Impact of an improved longwave radiation model, RRTM, on the energy budget and thermodynamic properties of the NCAR community climate model, CCM3. *J. Geophys. Res.*, **105**, 14 873–14 890, doi:10.1029/2000JD900091.

Janjić, Z. I., 1977: Pressure gradient force and advection scheme used for forecasting with steep and small scale topography. *Beitr. Phys. Atmos.*, **50**, 186–189.

Jiang, Q., 2003: Moist dynamics and orographic precipitation. *Tellus*, **55A**, 301–316, doi:10.3402/tellusa.v55i4.14577.

Jonkman, S. N., 2005: Global perspectives on loss of human life caused by floods. *Nat. Hazards*, **34**, 151–175, doi:10.1007/s11069-004-8891-3.

Joss, J., and R. Lee, 1995: The application of radar–gauge comparisons to operational precipitation profile corrections. *J. Appl. Meteor.*, **34**, 2612–2630, doi:10.1175/1520-0450(1995)034<2612:TAORCT>2.0.CO;2.

Kain, J. S., 2004: The Kain–Fritsch convective parameterization: An update. *J. Appl. Meteor.*, **43**, 170–181, doi:10.1175/1520-0450(2004)043<0170:TKCPAU>2.0.CO;2.

——, and J. M. Fritsch, 1993: Convective parameterization for mesoscale models: The Kain–Fritsch scheme. *The Representation of Cumulus Convection in Numerical Models*, *Meteor. Monogr.*, No. 24, Amer. Meteor. Soc., 165–170.

Katzfey, J. J., 1995a: Simulation of extreme New Zealand precipitation events. Part I: Sensitivity to orography and resolution. *Mon. Wea. Rev.*, **123**, 737–754, doi:10.1175/1520-0493(1995)123<0737:SOENZP>2.0.CO;2.

——, 1995b: Simulation of extreme New Zealand precipitation events. Part II: Mechanisms of precipitation development. *Mon. Wea. Rev.*, **123**, 755–775, doi:10.1175/1520-0493(1995)123<0755:SOENZP>2.0.CO;2.

Kitchen, M., and P. M. Jackson, 1993: Weather radar performance at long range—Simulated and observed. *J. Appl. Meteor.*, **32**, 975–985, doi:10.1175/1520-0450(1993)032<0975:WRPALR>2.0.CO;2.

Kushta, J., G. Kallos, M. Astitha, S. Solomos, C. Spyrou, C. Mitsakou, and J. Lelieveld, 2014: Impact of natural aerosols on atmospheric radiation and consequent feedbacks with the meteorological and photochemical state of the atmosphere. *J. Geophys. Res. Atmos.*, **119**, 1463–1491, doi:10.1002/2013JA019745.

Mahrer, Y., 1984: An improved numerical approximation of the horizontal gradients in a terrain-following coordinate system. *Mon. Wea. Rev.*, **112**, 918–922, doi:10.1175/1520-0493(1984)112<0918:AINAOT>2.0.CO;2.

Marchi, L., M. Borga, E. Preciso, and E. Gaume, 2010: Characterisation of selected extreme flash floods in Europe and implications for flood risk management. *J. Hydrol.*, **394**, 118–133, doi:10.1016/j.jhydrol.2010.07.017.

Medina, S., and R. A. Houze Jr., 2003: Air motions and precipitation growth in Alpine storms. *Quart. J. Roy. Meteor. Soc.*, **129**, 345–371, doi:10.1256/qj.02.13.

Meyers, M. P., R. L. Walko, J. Y. Harrington, and W. R. Cotton, 1997: New RAMS cloud microphysics parameterization. Part II: The two-moment scheme. *Atmos. Res.*, **45**, 3–39, doi:10.1016/S0169-8095(97)00018-5.

Mlawer, E. J., S. J. Taubman, P. D. Brown, M. J. Iacono, and S. A. Clough, 1997: Radiative transfer for inhomogeneous atmospheres: RRTM, a validated correlated-*k* model for the longwave. *J. Geophys. Res.*, **102**, 16 663–16 682, doi:10.1029/97JD00237.

Nicótina, L., E. Alessi Celegon, A. Rinaldo, and M. Marani, 2008: On the impact of rainfall patterns on the hydrologic response. *Water Resour. Res.*, **44**, W12401, doi:10.1029/2007WR006654.

Nikolopoulos, E. I., E. N. Anagnostou, M. Borga, E. R. Vivoni, and A. Papadopoulos, 2011: Sensitivity of a mountain basin flash flood to initial wetness condition and rainfall variability. *J. Hydrol.*, **402**, 165–178, doi:10.1016/j.jhydrol.2010.12.020.

——, N. S. Bartsotas, E. N. Anagnostou, and G. Kallos, 2015: Using high-resolution numerical weather forecasts to improve remotely sensed rainfall estimates: The case of the 2013 Colorado flash flood. *J. Hydrometeor.*, **16**, 1742–1751, doi:10.1175/JHM-D-14-0207.1.

NOAA/NCEP, 2000: NCEP FNL Operational Model Global Tropospheric Analyses, continuing from July 1999 (updated daily). NCAR Computational and Information Systems Laboratory Research Data Archive, accessed February 2015, doi:10.5065/D6M043C6.

Pellarin, T., G. Delrieu, G. M. Saulnier, H. Andrieu, B. Vignal, and J. D. Creutin, 2002: Hydrologic visibility of weather radar systems operating in mountainous regions: Case study for the Ardèche catchment (France). *J. Hydrometeor.*, **3**, 539–555, doi:10.1175/1525-7541(2002)003<0539:HVOWRS>2.0.CO;2.

Pielke, R. A., and Coauthors, 1992: A comprehensive meteorological modeling system RAMS. *Meteor. Atmos. Phys.*, **49**, 69–91, doi:10.1007/BF01025401.

Ponce, V. M., and R. H. Hawkins, 1996: Runoff curve number: Has it reached maturity? *J. Hydrol. Eng.*, **1**, 11–18, doi:10.1061/(ASCE)1084-0699(1996)1:1(11).

Reuter, H. I., A. Nelson, and A. Jarvis, 2007: An evaluation of void-filling interpolation methods for SRTM data. *Int. J. Geogr. Inf. Sci.*, **21**, 983–1008, doi:10.1080/13658810601169899.

Roberts, N. M., and H. W. Lean, 2008: Scale-selective verification of rainfall accumulations from high-resolution forecasts of convective events. *Mon. Wea. Rev.*, **136**, 78–97, doi:10.1175/2007MWR2123.1.

——, S. J. Cole, R. M. Forbes, R. J. Moore, and D. Boswell, 2009: Use of high-resolution NWP rainfall and river flow forecasts for advance warning of the Carlisle flood, north-west England. *Meteor. Appl.*, **16**, 23–34, doi:10.1002/met.94.

Rotunno, R., and R. Ferretti, 2001: Mechanisms of intense alpine rainfall. *J. Atmos. Sci.*, **58**, 1732–1749, doi:10.1175/1520-0469(2001)058<1732:MOIAR>2.0.CO;2.

——, and R. A. Houze, 2007: Lessons on orographic precipitation from the Mesoscale Alpine Programme. *Quart. J. Roy. Meteor. Soc.*, **133**, 811–830, doi:10.1002/qj.67.

Sangati, M., and M. Borga, 2009: Influence of rainfall spatial resolution on flash flood modelling. *Nat. Hazards Earth Syst. Sci.*, **9**, 575–584, doi:10.5194/nhess-9-575-2009.

——, ——, D. Rabuffetti, and R. Bechini, 2009: Influence of rainfall and soil properties spatial aggregation on extreme flash flood response modelling: An evaluation based on the Sesia River basin, north western Italy. *Adv. Water Resour.*, **32**, 1090–1106, doi:10.1016/j.advwatres.2008.12.007.

Schwartz, C. S., 2014: Reproducing the September 2013 record-breaking rainfall over the Colorado Front Range with high-resolution WRF forecasts. *Wea. Forecasting*, **29**, 393–402, doi:10.1175/WAF-D-13-00136.1.

——, and Coauthors, 2009: Next-day convection-allowing WRF Model guidance: A second look at 2-km versus 4-km grid spacing. *Mon. Wea. Rev.*, **137**, 3351–3372, doi:10.1175/2009MWR2924.1.

Simonović, S. P., 2003: *Floods in a Changing Climate: Risk Management.* Cambridge University Press, 194 pp.

Sinclair, M. R., D. S. Wratt, R. D. Henderson, and W. R. Gray, 1997: Factors affecting the distribution and spillover of precipitation in the Southern Alps of New Zealand—A case study. *J. Appl. Meteor.*, **36**, 428–442, doi:10.1175/1520-0450(1997)036<0428:FATDAS>2.0.CO;2.

Smith, R., and Coauthors, 1997: Local and remote effects of mountains on weather: Research needs and opportunities. *Bull. Amer. Meteor. Soc.*, **78**, 877–892.

Solomos, S., G. Kallos, J. Kushta, M. Astitha, C. Tremback, A. Nenes, and Z. Levin, 2011: An integrated modeling study on the effects of mineral dust and sea salt particles on clouds and precipitation. *Atmos. Chem. Phys.*, **11**, 873–892, doi:10.5194/acp-11-873-2011.

Taylor, K. E., 2001: Summarizing multiple aspects of model performance in a single diagram. *J. Geophys. Res.*, **106**, 7183–7192, doi:10.1029/2000JD900719.

USDA, 1986: Urban hydrology for small watersheds. Tech. Release 55, 164 pp. [Available online at https://www.nrcs.usda.gov/Internet/FSE_DOCUMENTS/stelprdb1044171.pdf.]

Weckwerth, T. M., and D. B. Parsons, 2006: A review of convection initiation and motivation for IHOP_2002. *Mon. Wea. Rev.*, **134**, 5–22, doi:10.1175/MWR3067.1.

——, L. J. Bennett, L. J. Miller, J. Van Baelen, P. Di Girolamo, A. M. Blyth, and T. J. Hertneky, 2014: An observational and modeling study of the processes leading to deep, moist convection in complex terrain. *Mon. Wea. Rev.*, **142**, 2687–2708, doi:10.1175/MWR-D-13-00216.1.

Wulfmeyer, V., and Coauthors, 2011: The Convective and Orographically-Induced Precipitation Study (COPS): The scientific strategy, the field phase, and research highlights. *Quart. J. Roy. Meteor. Soc.*, **137**, 3–30, doi:10.1002/qj.752.

Zhang, X., E. N. Anagnostou, M. Frediani, S. Solomos, and G. Kallos, 2013: Using NWP simulations in satellite rainfall estimation of heavy precipitation events over mountainous areas. *J. Hydrometeor.*, **14**, 1844–1858, doi:10.1175/JHM-D-12-0174.1.

Zoccatelli, D., M. Borga, A. Viglione, G. B. Chirico, and G. Bloschl, 2011: Spatial moments of catchment rainfall: Rainfall spatial organisation, basin morphology, and flood response. *Hydrol. Earth Syst. Sci.*, **15**, 3767–3783, doi:10.5194/hess-15-3767-2011.